



ELSEVIER

Contents lists available at ScienceDirect

## Data in Brief

journal homepage: [www.elsevier.com/locate/dib](http://www.elsevier.com/locate/dib)



### Data Article

# Characterization of mineral coatings associated with a Pleistocene-Holocene rock art style: The Northern Running Figures of the East Alligator River region, western Arnhem Land, Australia



Penelope L. King<sup>a,\*</sup>, Ulrike Troitzsch<sup>a</sup>, Tristen Jones<sup>b</sup>

<sup>a</sup> Research School of Earth Sciences, The Australian National University, Canberra, ACT 2601, Australia

<sup>b</sup> Department of Archaeology and Natural History, School of Culture, History and Language, The Australian National University, Canberra, ACT 2601, Australia

#### ARTICLE INFO

##### Article history:

Received 8 November 2016

Received in revised form

9 December 2016

Accepted 13 December 2016

Available online 20 December 2016

##### Keywords:

X-ray Diffraction

Scanning Electron Microscopy energy dispersive spectroscopy

Fourier Transform infrared spectroscopy

#### ABSTRACT

This data article contains mineralogic and chemical data from mineral coatings associated with rock art from the East Alligator River region. The coatings were collected adjacent to a rock art style known as the “Northern Running Figures” for the purposes of radiocarbon dating (<http://dx.doi.org/10.1016/j.jasrep.2016.11.016>; (T. Jones, V. Levchenko, P.L. King, U. Troitzsch, D. Wesley, 2017) [1]). This contribution includes raw and processed powder X-ray Diffraction data, Scanning Electron Microscopy energy dispersive spectroscopy data, and Fourier Transform infrared spectral data.

© 2016 The Authors. Published by Elsevier Inc. This is an open access article under the CC BY license

(<http://creativecommons.org/licenses/by/4.0/>).

DOI of original article: <http://dx.doi.org/10.1016/j.jasrep.2016.11.016>

\* Corresponding author.

E-mail address: [penny.king@anu.edu.au](mailto:penny.king@anu.edu.au) (P.L. King).

<http://dx.doi.org/10.1016/j.dib.2016.12.024>

2352-3409/© 2016 The Authors. Published by Elsevier Inc. This is an open access article under the CC BY license (<http://creativecommons.org/licenses/by/4.0/>).

## Specifications Table

Subject area	Archeology
More specific subject area	Rock art
Type of data	Tables and Figures
How data was acquired	<ol style="list-style-type: none"> <li>1. Powder X-ray diffraction (XRD) analysis (PANalytical Empyrean powder X-ray diffractometer, Research School of Chemistry, Australian National University)</li> <li>2. Scanning Electron Microscope energy dispersive spectral (SEM-EDS) analysis (Hitachi 4300SE/N field emission scanning electron microscope equipped with an Oxford INCA Energy 350 EDS system at the Centre for Advanced Microscopy, Australian National University)</li> <li>3. Fourier Transform Infrared (FTIR) spectroscopic analysis – mid-infrared spectral range (Bruker Tensor 27, Research School of Earth Sciences, Australian National University)</li> </ol>
Data format	Raw and analysed
Experimental factors	Characterization of mineralogy and chemistry of mineral coatings associated with rock art
Experimental features	Analysis of minerals, their quantities and their chemical composition
Data source location	Eastern Alligator River, western Arnhem Land, Australia
Data accessibility	The data is available with this article.

## Value of the data

- Data presented here will be useful to other researchers as a benchmark for Powder X-ray Diffraction and Fourier Transform Infrared spectra of natural oxalate-bearing mineral coatings.
- The raw XRD data may be reanalyzed with a different set of phosphate, sulfate and oxalate standards, which may help constrain the uncertainty in the Rietveld refinement values.
- The raw FTIR data may be deconvolved using other appropriate mineral databases and the results compared with the XRD Rietveld refinement values.

## 1. Data

### 1.1. Data from X-ray diffraction with Rietveld refinement fits

The oxalate mineral, whewellite, is found in all mineral crusts sampled (13–26.4 wt.%), except RLL3-1-1 where it is not detected (Table 1, Supplementary Figs. 1 and 2, Supplementary Table 1). Samples RLL32-B-S1 to RLL32-B-S4, RLL3-1-2 and RLL3-1-3 have the same mineral assemblage: whewellite and tinsleyite, with lesser taranakite, quartz and gypsum (Table 1). Sample RLL32-B-2011 is dominated by quartz and whewellite, with a little gypsum, a 10 Å-mica and a 7.1 Å-clay. Sr-crandallite or goyazite may be present at low levels (Table 1).

### 1.2. Data from Scanning Electron Microscope analysis

Backscattered electron (BSE) imaging data (Fig. 8a and 8d in [1]) indicates that the mineral crust contains at least four intimately mixed minerals (< 1 µm to ~3 µm). As shown in Table 2, SEM-EDS data from the mineral crust indicates whewellite, and Ca–Al–(Sr)–phosphate(s) –crandallite, Sr-crandallite, or crandallite mixed with apatite.

**Table 1**

Quantitative data for minerals in the crusts based on Rietveld refinement fits of X-ray diffraction data.

Sample	RLL032-B-2011	RLL032-B-S1	RLL032-B-S2	RLL032-B-S3	RLL032-B-S4	RLL3-1-1	RLL3-1-2	RLL3-1-3
<b>Scan No.</b>	A24950	A25292	A25302	A25301	A25290	A24950	A25292	A25302
<b><math>R_{wp}</math><sup>a</sup></b>	4.53	4.63	3.28	3.40	3.70	4.75	4.09	4.30
<b>Mineral- wt.%( <i>sd</i>)<sup>b</sup></b>								
Amorphous material	70.5 (5.0)	53.8 (5.0)	52.3 (5.0)	65.9 (5.0)	69.5 (5.0)	28.3 (3.0)	14.9 (3.0)	40.6 (5.0)
Quartz SiO <sub>2</sub>	9.3 (0.7)	2.5 (0.1)	3.1 (0.1)	2.9 (0.2)	1.7 (0.2)	32.7 (0.6)	5.6 (0.3)	3.2 (0.2)
Gypsum CaSO <sub>4</sub> ·2H <sub>2</sub> O	1.1 (0.2)	3.7 (0.3)	3.0 (0.3)	0.8 (0.2)	1.7 (0.2)	1.8 (0.1)	3.1 (0.2)	2.0 (0.1)
Whewellite CaC <sub>2</sub> O <sub>4</sub> ·H <sub>2</sub> O	13.0 (0.9)	20.3 (0.8)	20.1 (0.7)	17.4 (0.8)	15.1 (0.9)		26.4 (0.6)	17.4 (0.6)
Tinsleyite KAl <sub>2</sub> (PO <sub>4</sub> ) <sub>2</sub> (OH)·2H <sub>2</sub> O		17.7 (1.0)	18.2 (0.8)	12.9 (0.8)	11.9 (0.9)	21.5 (0.5)	48.3 (0.8)	35.2 (0.9)
Taranakite K <sub>3</sub> Al <sub>5</sub> (HPO <sub>4</sub> ) <sub>6</sub> (PO <sub>4</sub> ) <sub>2</sub> ·18H <sub>2</sub> O		2.1 (0.1)	3.4 (0.3)	0.1 (0.2)	0.2 (0.2)	0.3 (0.1)	1.8 (0.2)	1.6 (0.3)
Goyazite SrAl <sub>3</sub> P <sub>2</sub> O <sub>7</sub> (OH) <sub>7</sub>	1.5 (0.4)							
7.1 Å-clay <sup>c</sup>	0.8 (0.4)							
10 Å-mica <sup>c</sup>	3.8 (0.6)							
Variscite AlPO <sub>4</sub> ·2H <sub>2</sub> O						15.4 (0.4)		
<b>Total</b>	<b>100</b>	<b>100</b>	<b>100</b>	<b>100</b>	<b>100</b>	<b>100</b>	<b>100</b>	<b>100</b>

<sup>a</sup> Goodness-of-fit indicator  $R_{wp}$  for the weighted profile:  $R_{wp} = [(\sum w_i(y_{io} - y_{ic})^2) / (\sum w_i y_{io}^2)]^{1/2}$ , where  $y_{io}$  is the observed intensity,  $y_{ic}$  the calculated intensity, and  $w_i$  the weight assigned to each observation based on counting statistics.

<sup>b</sup> Refined variables included zero correction, scale factors, unit cell parameters of major phases and up to four peak shape parameters per mineral.

<sup>c</sup> 7.1 Å-clay is likely kaolinite and 10 Å-mica is likely illite or muscovite.

### 1.3. Data from Fourier Transform Infrared spectroscopy

Fourier Transform Infrared spectra provide constraints for the presence of oxalates, sulfates, phosphates and clay minerals in the crusts (Fig. 1a and b). Infrared bands associated with the calcium oxalate (whewellite) are evident in the spectra at 1315–1320 and 780 (C<sub>2</sub>O<sub>4</sub>) and 670 cm<sup>-1</sup> (water libration) and possible bands include 1430 cm<sup>-1</sup> (C<sub>2</sub>O<sub>4</sub>), 3420 cm<sup>-1</sup> (OH), and 1625 cm<sup>-1</sup> (HOH). Phosphate minerals (crandallite, Sr-crandallite/goyazite and apatite) have bands at 1383, ~1110 and 890 cm<sup>-1</sup> and 1020 cm<sup>-1</sup> related to PO<sub>4</sub> vibrations and 3486 cm<sup>-1</sup> related to OH. Bands due to silicate minerals are found at 3246 cm<sup>-1</sup> (Al<sub>2</sub>-OH, clay) and 1020 cm<sup>-1</sup> (SiO<sub>4</sub>). The FTIR data does not rule out sulfate (Supplementary Table 2). Bands at 3344 and 3062 cm<sup>-1</sup> are assigned to OH groups in minerals.

The six FTIR spectra obtained from the RLL032B-B site ([1], Fig. 1a) are consistent with one another with only slight differences observed in the topmost sample (RLL032-B-2011). The latter shows slightly less defined OH bands at 3490–3420 cm<sup>-1</sup> and a doublet in the area near 670 cm<sup>-1</sup>. The FTIR data is consistent with the XRD that shows that RLL032-B-2011 differs from the rest of the samples (Fig. 1a).

RLL3-1-2 and RLL3-1-3 both contain strong oxalate bands, phosphate bands and H–O molecular species (Fig. 1b). RL3-1-1 does not show detectable oxalate, but instead contains bands between 1000–1100 cm<sup>-1</sup> and 1800–2100 cm<sup>-1</sup> (Fig. 1b) due to Al–O and Si–O vibrations (e.g. variscite and quartz; Table 1, Supplementary Table 2).

**Table 2**  
SEM-EDS analyses of the phases and mixed phases in RL32-B-2011.

Mineral	Whewellite		Crandallite	Sr crandallite	Crandallite
<b>SEM analysis of</b>	> 1 phase	> 1 phase	1 phase	1 phase	> 1 phase
<b>Analysis #</b>	#15	#7	#1	#26	#13
<b>wt% (norm C free)</b>					
SiO <sub>2</sub>	6.5	5.22	0	0.2	2.42
Al <sub>2</sub> O <sub>3</sub>	5.15	7.09	42.83	37.73	8.17
FeO	1.29		1.08	0.27	
MgO	0	0	0.01	0	0
CaO	79.36	68.48	9.87	11.23	43.65
SrO				11.14	
Na <sub>2</sub> O	0.74	1.13	0.57	0	1.23
K <sub>2</sub> O	1.25	3.9	1.41	0.19	2.62
P <sub>2</sub> O <sub>5</sub>	5.37	11.06	37.56	29.64	39.51
SO <sub>3</sub>	0	2.5	6.35	9.52	1.11
Cl	0.35	0.62	0.32	0.08	1.29
<b>Atomic formula unit, based on:</b>	<b>4 O + 2 C</b>	<b>4 O + 2 C</b>	<b>13 O</b>	<b>13 O</b>	<b>11 O</b>
Si	0.21	0.17	0	0.02	0.17
Al	0.2	0.27	3.84	3.8	0.69
Fe total	0.04	0	0.07	0.02	0
Mg	0	0	0	0	0
Ca	1.40*	1.18*	0.8	1.03	3.34
Sr				0.55	
Na	0.05	0.07	0.08	0	0.17
K	0.05	0.16	0.14	0.02	0.24
P	0.15	0.3	2.42	2.14	2.39
Cl	0.02	0.03	0.04	0.01	0.16
<b>TOTAL</b>	1.95	1.84	4.82	5.23	4.59
<b>Ideal Formula</b>	CaC <sub>2</sub> O <sub>4</sub> ·H <sub>2</sub> O		CaAl <sub>3</sub> (PO <sub>4</sub> ) <sub>2</sub> (OH) <sub>5</sub> ·H <sub>2</sub> O	(Ca,Sr)Al <sub>3</sub> (PO <sub>4</sub> ) <sub>2</sub> (OH) <sub>5</sub> ·H <sub>2</sub> O	Ca <sub>3</sub> Al(PO <sub>4</sub> ) <sub>2</sub> (OH) <sub>3</sub> ·H <sub>2</sub> O
<b>Measured Formula</b>			Ca <sub>0.8</sub> Al <sub>3.84</sub> (PO <sub>4</sub> ) <sub>2.42</sub> (OH) <sub>5</sub> ·H <sub>2</sub> O	(Ca,Sr) <sub>1.58</sub> Al <sub>3.8</sub> (PO <sub>4</sub> ) <sub>2.14</sub> (OH) <sub>5</sub> ·H <sub>2</sub> O	

## 2. Experimental design, materials and methods

### 2.1. Study area description

Mineral coatings were collected from rock walls adjacent to art described in detail by [1]. The locations are given in Table 3.

### 2.2. X-ray diffraction (XRD) methods

Samples were prepared as powders, mounted on a silicon low-background sample holder, and analyzed from 4 to 70° 2θ at a spacing of 0.02626° (Supplementary Table 1). Data was collected using Bragg Brentano geometry, fixed divergence slits with Cu Kα radiation and a PIXcel 1D detector (active length = 3.3473°, 255 channels, 542 s per step). Minerals were identified using the SIEMENS software package *Diffraclus* Eva 10 [2] (Supplementary Fig. 1) and quantified using Rietveld refinement [3,4] with the program *Rietica* [5] (Table 1, Supplementary Fig. 2). The background was fixed manually. The weight fraction of the amorphous material  $W_{AMORPH}$  was determined for each corundum-spiked

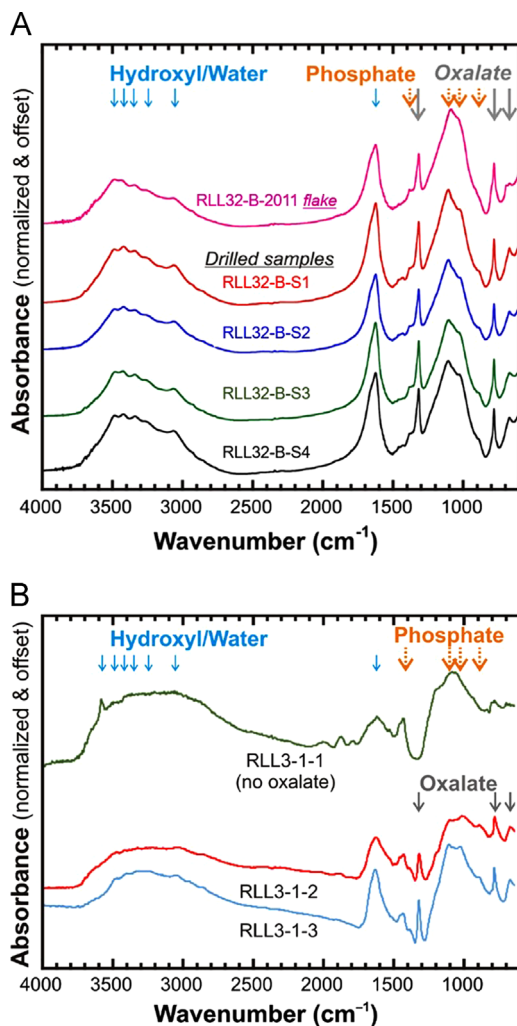


**Fig. 1.** FTIR spectra of bulk samples from the mineral crusts. The positions of the bands identified in [Supplementary Table 2](#) are indicated. (A) RLL032-B powders. (B) RLL3-1 powders. RLL3-1-1 does not contain detectable oxalate.

**Table 3**  
Sample identification and location.

Sample	Latitude	Longitude
RLL032-B-2011	12°23'49.55"S	133° 0'26.81"E
RLL032-B-S1	12°23'49.55"S	133° 0'26.81"E
RLL032-B-S2	12°23'49.55"S	133° 0'26.81"E
RLL032-B-S3	12°23'49.55"S	133° 0'26.81"E
RLL032-B-S4	12°23'49.55"S	133° 0'26.81"E
RLL3-1-1	12°24'7.59"S	133° 0'5.51"E
RLL3-1-2	12°24'7.59"S	133° 0'5.51"E
RLL3-1-3	12°24'7.59"S	133° 0'5.51"E

sample according to equation  $W_{AMORPH}=1-y/x$ , where  $y=\%$  corundum, and  $x$  is the calculated % corundum given by the program Rietica [6]. Amorphous, poorly crystallized and/or very finely grained material is identified in all samples by elevated or undulating backgrounds.

### 2.3. Scanning electron microscopy – energy dispersive spectrometry (SEM-EDS) methods

Sample RLL032-B-2011 was mounted in epoxy perpendicular to the mineral crust surface and polished to a  $\frac{1}{4}$   $\mu\text{m}$  diamond grit finish using kerosene, not water. SEM analysis was undertaken using a 15 kV accelerating voltage and 1 nA beam current with an approximately 2  $\mu\text{m}$  beam diameter that overlapped multiple mineral phases.

### 2.4. Fourier Transform Infrared (FTIR) spectroscopy methods

Samples were ground, dried at  $\sim 100$  °C, and mixed with KBr (sample:KBr = 0.6:1) and pressed into a 3 mm diameter disc held in a paper holder. Spectra were collected using a Bruker Tensor 27 with a Globar source, KBr beamsplitter and DTGS detector in transmission mode under a dry air purge from 400 to at least 4000  $\text{cm}^{-1}$ , with 4  $\text{cm}^{-1}$  resolution and 100 scans. (Supplementary Table 3). FTIR bands were located using the OPUS software (v8.0) provided by Bruker and identified using data from the literature (Supplementary Table 2, [7–10]).

## Acknowledgements

This research was supported by Australian Research Council grants to King (FT130101524 and DP150104604). The Centre for Advanced Microscopy is supported by the Australian Microscopy and Microanalysis Research Facility (AMMRF). We thank Lasse Noren from the Research School of Chemistry, Australian National University for assistance with the X-ray diffraction data collection.

## Transparency document. Supporting information

Transparency data associated with this article can be found in the online version at <http://dx.doi.org/10.1016/j.dib.2016.12.024>.

## Appendix A. Supporting information

Supplementary data associated with this article can be found in the online version at <http://dx.doi.org/10.1016/j.dib.2016.12.024>.

## References

- [1] T. Jones, V. Levchenko, P.L. King, U. Troitzsch, D. Wesley, Radiocarbon age constraints for a Pleistocene – Holocene transition rock art style: the Northern Running Figures of the East Alligator River region, western Arnhem Land, Australia, *J. Archeol. Sci. Rpt.* 11 (2017) 80–89. <http://dx.doi.org/10.1016/j.jasrep.2016.11.016>.
- [2] Bruker, DIFFRACplus BASIC Evaluation Package EVA 10.0, User's Manual, Bruker AXS GmbH, Karlsruhe, Germany, 2004.
- [3] H.M. Rietveld, Line profiles of neutron powder-diffraction peaks for structure refinement, *Acta Crystall* 22 (1967) 151–152.
- [4] H.M. Rietveld, A profile refinement method for nuclear and magnetic structures, *J. Appl. Cryst.* 2 (1969) 65–71.
- [5] B. Hunter, Rietica – a visual Rietveld program, *IUCR Comm. Powder Diffract. News* 20 (1998) 21.
- [6] Sietronics, Siroquant Technical Manual, Sietronics Pty Ltd: Mitchell, ACT, Australia, 2006.
- [7] H.W. van der Marel, H. Beutelspacher, *Atlas of Infrared Spectroscopy of Clay Minerals and Their Admixtures*, Elsevier Sci Publ Co, Amsterdam, 1976.

- [8] P. Maravelaki-Kalaitzaki, Black crusts and patinas on Pentelic marble from the Parthenon and Erechtheum (Acropolis, Athens): characterization and origin, *Anal. Chim. Acta* 532 (2005) 187–198.
- [9] S. Marincea, D. Dumitras, R. Gilbert, Tinsleyite in the "dry" Cioclovina Cave Sureanu Mountains, Romania: the second occurrence, *Eur. J. Mineral.* 14 (2002) 157–164.
- [10] S. Weiner, P. Goldberg, O. Bar-Yosef, Three-dimensional distribution of minerals in the sediments of Hayonim Cave, Israel: diagenetic processes and archeological implications, *J. Arch. Sci.* 29 (2002) 1289–1308.